Journal of Medicinal Chemistry

Article

Structure-based Tetravalent Zanamivir with Potent Inhibitory Activity against Drug-resistant Influenza Viruses

Lifeng Fu, Yuhai Bi, Yan Wu, Shanshan Zhang, Jianxun Qi, Yan Li, Xuancheng Lu, Zhenning Zhang, Xun Lv, Jinghua Yan, George F. Gao, and Xuebing Li

J. Med. Chem., **Just Accepted Manuscript** • DOI: 10.1021/acs.jmedchem.6b00537 • Publication Date (Web): 24 Jun 2016

ACS Publications

Journal of Medicinal Chemistry is published by the American Chemical Society. 1155 Sixteenth Street N.W., Washington, DC 20036

Structure-based Tetravalent Zanamivir with Potent Inhibitory Activity against Drug-resistant Influenza Viruses

Lifeng Fu,[†,‡,▽,⊥] Yuhai Bi,[†,⊥] Yan Wu,[†,⊥] Shanshan Zhang,[†,▽] Jianxun Qi,[†] Yan Li,[†] Xuancheng Lu,[§] Zhenning Zhang,[†,▽] Xun Lv,[†] Jinghua Yan,[†,#] George F. Gao,*[,†,#] and Xuebing Li*[,†,‡,#]

[†]CAS Key Laboratory of Pathogenic Microbiology and Immunology, Institute of Microbiology, Chinese Academy of Sciences, Chaoyang District, Beijing 100101, China

[‡]National Engineering Research Center for Carbohydrate Synthesis, Jiangxi Normal University, Nanchang 330022, China

[▽]Graduate University of Chinese Academy of Sciences, Shijingshan District, Beijing 100049, China

[§]Laboratory Animal Center, Chinese Center for Disease Control and Prevention, Changping District, Beijing 102206, China

[#]Center for Influenza Research and Early-warning, Chinese Academy of Sciences (CASCIRE), Chaoyang District, Beijing 100101, China

ABSTRACT: Zanamivir and oseltamivir are principal influenza antiviral drugs that target viral neuraminidase (NA), but resistant viruses containing mutant NAs with diminished drug affinity are increasingly emerging. Using the structural knowledge of both drug-binding sites and their spatial arrangement on the homotetrameric NA, we have developed a tetravalent zanamivir (TZ) molecule that exhibited marked increases in NA binding affinity, inhibition of NA enzyme activity, and in vitro plus in vivo antiviral efficacy over zanamivir. TZ functioned against both human seasonal

H3N2 and avian H7N9 viruses, including drug-resistant mutants. Crystal structure of a resistant N9 NA in complex with TZ explained the function, which showed that four zanamivir residues simultaneously bound to all four monomers of NA. The design method of TZ described in this study may be useful to develop drugs or ligands that target proteins with multiple binding sites. The potent anti-influenza activity of TZ makes it attractive for further development.

INTRODUCTION

Influenza neuraminidase (NA) is a homotetrameric enzyme on the viral envelope, and hydrolyzes sialic acids from glycan receptors on the host cells to enable the release and spread of progeny virus from the infected cells.[1] Anti-influenza drugs, zanamivir (ZNV) and oseltamivir (OSV), are two structural analogues of sialic acid in the catalytic transition state (Figure 1) that interact with the NA active site more potently than the natural substrate, thereby reducing virus propagation.[2,3] As the amino acid residues within and near the active site are highly conserved, ZNV and OSV are effective against all influenza A and B viruses.[4] However, drug-resistant mutations have been increasingly identified in the NA of various strains, including human seasonal H3N2 and H1N1 viruses, and avian H5N1 and H7N9 viruses that are capable of infecting humans.[5−10] Evidence suggests that the mutations compromise the interaction between NA and drugs, although they retain the ability to engage the active site.[11,12] Functional group modification of ZNV or OSV[13−18] and exploration of a structurally new NA inhibitor[19−23] may antagonize drug resistance. Synthetic conjugates that contain multiple copies of an inhibitor displayed on appropriate scaffolds,[24−29] as typically illustrated by a series of divalent zanamivir derivatives,[26−28] can also increase antiviral activity. However, because the multivalent inhibitors described so far were designed without consideration of spatial

arrangement of the active sites on the tetrameric NA molecules, the activity gain is largely a consequence of their ability to induce virus aggregation on the host cell surface, rather than the cause of an increase in the intrinsic binding affinity.[26,28]

RESULTS AND DISCUSSION

The crystal structures of NA show that four active sites are symmetrically arranged on the top surface of the NA tetramer with a spacing of ~38 Å from the center of symmetry.[30,31] The exposed radial arrangement of the sites is thermodynamically favorable for oligovalent-ligand bindings, as seen for the pentameric Shiga-like toxin[32,33] and the trimeric adenovirus fiber protein.[34] On the basis of these findings, we designed a set of conjugated molecules, in which four terminal ZNV residues were anchored on a small central scaffold by oligoethylene glycol (OEG) linkers of different lengths (Figure 1D). We anticipated that compound **1**, with a molecular dimension complementary to the distribution of NA binding sites, might occupy all the sites of a NA molecule and therefore dramatically improve its intrinsic binding affinity through the decreased binding energy. To develop a putatively potent NA inhibitor, we took into account three essential parameters when designing the TZs. First, an easily accessible and chemically symmetric tetraazide (**16**, Scheme 1) served as the scaffold, from which four ZNV residues radiated out to engage all NA subunits. Second, ZNV but not OSV was chosen as the pharmacophore, because ZNV is structurally more similar to the natural NA substrate, and therefore the viral resistance to ZNV occurs less frequently.[11] In addition, all functional groups around the cyclohexene core of OSV are involved in the interaction with the NA active site,[3] whereas in the enzyme-bound state, the 7-hydroxyl group of ZNV is oriented toward the outside of the site and makes no virtual contact with the enzyme.[2] This provided the best connection

point for tethering ZNV pharmacophores with minimized impairment of the binding affinity. Finally, a flexible OEG linker (**9**, **10**, or **11**) was used to bridge the pharmacophores and the scaffold, with its beneficial pharmacological properties[35] contributing to the resistance to nonspecific binding and metabolic clearance, as well as the aqueous solubility of the large TZs.

Using the known crystal structure of an N9 NA,[12] our molecular modelling study predicted that compound **1** would attach to the protein surface, through the four ZNV residues binding simultaneously to the active sites (Figure 1E). The calculated free energy of **1** binding to NA (−111 kcal mol^{-1}) is markedly lower than that of ZNV binding (−58 kcal mol^{-1}), suggesting that a substantial affinity increase may be achieved using such a complemented oligovalent interaction. We then synthesized **1**, as well as the controls **2** and **3**, to perform functional and mechanistic studies. A concise modular strategy[29] that accommodated the above-mentioned design elements was used to yield synthetic assemblies. Nucleophilic substitution of a 7-activated ZNV derivative (**12**) by an amine-terminated OEG (**9**, **10**, or **11**) accomplished coupling between the pharmacophore and the linker. The alkyne functionality at the other end of the linker allowed the straightforward installation of the pharmacophores onto the scaffold **16** through the use of a Cu(I)-catalyzed Huisgen cycloaddition reaction.[36] All resulting TZs showed excellent aqueous solubility (≥1.0 M), and were fully characterized by HPLC (purity > 95%), NMR, and mass spectroscopy.

We cloned four recombinant influenza NAs: a N2 and its mutant (mutN2) from H3N2 A/Moscow/10/99, and two N9s from H7N9 A/Anhui/1/2013 (anhN9) and H7N9 A/Shanghai/2/2013 (shaN9), respectively. These soluble proteins were prepared through a baculovirus−insect cell expression system[12,19,37−42] and were used as models to examine the interactions with TZs. The N2 is a common NA serotype found in seasonal and pandemic H3N2 viruses and the N9 represents a

serotype found in emerging avian H7N9 viruses that can cause fatal infection in humans. The mutN2 carries E119V and I222L dual substitutions (N2 numbering) and the shaN9 has an R294K replacement relative to anhN9 (N9 numbering). These mutations lie within the NA active site and are known to confer resistance to OSV and ZNV.[12,43] In the assays using a fluorescent substrate[12,19,38] to measure the inhibition of NA enzyme activity, all TZs exhibited potent efficacies for the test NAs (Figure 2A−D). In each case compound **1** showed a higher activity than other TZs and this superiority became more evident for the inhibition of drug-resistant mutN2 and shaN9. Similarly, compound **1** had a similar efficacy to ZNV for the inhibition of the drug-sensitive N2 and anhN9, whereas for the resistant NAs, it retained a low- or sub-nanomolar potency that was at least 6-fold higher than that of ZNV. Additionally, an octavalent ZNV conjugate (**25**, Scheme 2), which has a central scaffold and OEG linkers similar to those of TZs, was less effective than compound **1** for the inhibition of all tested enzymes. This result demonstrates that the increased multivalency could not result in further improvement in the activity.

Surface plasmon resonance (SPR) experiments showed that TZs and ZNV bound to both N2 and mutN2 NAs, with the responses proportional to their molecular masses (Figure 2E). In contrast, no interaction was detected between TZs and bovine serum albumin (BSA) or between the NAs and a tetravalent OEG backbone molecule (**29**) that contained no ZNV residues (for the structure of **29**, see Scheme 2; for the SPR sensorgrams, see Figure S1 in the Support Information). This confirmed that the ZNV residues of TZs were responsible for the observed specific binding. In almost all cases, TZs showed slightly slower association rates (k_{on}) than ZNV, consistent with the increased molecular size that hampers motility. TZs also showed reduced dissociation rates (k_{off}). In particular, the decreases in the k_{off} value of **1** were significant, which resulted in an approximate picomolar affinity

(K_D) for both NAs, strongly suggesting that this molecule could interact with NAs to form highly stable complexes. As the known divalent[26,28] and tetravalent[25,29] ZNV derivatives, of which the molecular dimension does not match the distribution of NA active sites, generally showed a lower NA affinity (or NA-inhibitory activity) than ZNV, the binding kinetic analysis of compound **1** further reinforce the hypothesis that a marked increase in affinity could be generated through a complemented multiple interaction. In addition, although it is difficult to directly correlate the binding kinetics to the enzyme inhibition of TZs because of the different assay formats, the enhancement in both the affinity (K_D) and efficacy (IC_{50}) of **1** compared to those of ZNV were more markedly observed for the drug-resistant NA than the sensitive NA.

We solved the crystal structure of shaN9 NA in complex with compound **1** to explore the structural basis for the improved efficacy and affinity. The crystal diffracted to high resolution with clear electron density showing that four ZNV residues connected to a short part of the linker were trapped on the tetramer surface (Figure 2F and Figure S2). All the ZNV residues interacted with the NA active sites in an identical manner to that of ZNV bound by the same enzyme[12] (Figure S3), and the multiple bindings did not disrupt the tetramer structure. However, as the central part of the linker and the scaffold were undetectable by crystallography owing to their flexibility and incompetence in making direct contact with the enzyme, it was unclear whether these ZNV residues belong to a single tetravalent molecule. To address this issue, we performed analytical ultracentrifugation (AUC) experiments and revealed that the addition of compound **1** at different concentrations to the shaN9 tetramer in solution did not result in apparent intermolecular cross-links (Figure 3). This indicated that the observed complex by crystallography was formed through a 1:1 binding of **1** to the shaN9 tetramer, and that the formation of this complex should be thermodynamically more preferable than

that of intermolecular bridges. These findings explain the mechanism behind the remarkable ability of compound **1** to bind and inhibit the enzyme.

To evaluate the therapeutic potential of compound **1**, we examined its antiviral activity in Madin-Darby canine kidney (MDCK) cells. Four viruses, which contain N2, mutN2, anhN9, and shaN9 NAs, respectively, were rescued with reverse genetics[12,42,44−46] and were used for assays (Table 1). In agreement with its IC_{50} against enzymes (Figure 2A−D), compound **1** inhibited viral replication more potently than ZNV, with efficacies (EC_{50}) in the low-nanomolar range even against the drug-resistant viruses. To ensure that the improved antiviral activity did not simply result from the increased multivalency or steric hindrance, compounds **25** and **29** were tested as controls. Octavalent **25** had a similar efficacy to **1**, and the backbone molecule **29** showed no antiviral effect. In addition, transmission electron microscopy (TEM) examination of the H3N2 virus after incubation with **1** demonstrated that the tetravalent inhibitor was unable to induce viral aggregation (Figure 4 and Figure S4). This is in marked contrast to the divalent ZNV derivative that can bridge virus particles through interviral NA bindings.[26,28] The different binding modes of these two inhibitors could be attributed to their structural features. The divalent compound, which has an 18-atom linker (corresponding to ~23 Å in length) to join two ZNV residues, is incapable of simultaneous engagement to multiple sites within a NA molecule and, therefore, the binding to the NAs on different virions occurs. This mechanism of action is also proposed to contribute to the increased antiviral activity of the known tetravalent ZNV derivatives.[25,29] The sensitivity of virus replication in cell cultures to the inhibitors is influenced by multiple factors besides NA, such as viral fitness and assay process. This makes it difficult to clearly explain how the measured values of IC_{50} and K_D (Figure 2) can be translated to those of EC_{50} (Table 1). However, the TEM result, together with the

crystallographic and AUC studies, suggested that the potent in vitro antiviral activity of **1** is associated with its strong binding to a single NA molecule on the viral surface.

We next assessed the efficacy of compound **1** in mice that were challenged with a laboratory-adapted influenza viral strain, A/Puerto Rico/8/34 (H1N1). A preliminary test to evaluate the in vitro effect of inhibitors against this virus in a MDCK cell culture, showed that **1** exhibited an activity lower than 4 nM, which was more than 25 times as potent as ZNV (Figure S5). In addition, compound **1** demonstrated a mean half-life ($T_{1/2}$) of 72 min in an intravenous pharmacokinetic study in rats (Table S4). Although the rapid clearance of **1** from the circulation was over 2-fold longer than ZNV ($T_{1/2}$ = 32 min), this convinced us that an oral or subcutaneous route of administration was unlikely to provide efficient protection to mice against a lethal viral infection. The infected mice were therefore treated intranasally with the inhibitors, in a similar manner to the inhaled ZNV in clinical use, which delivers the drug directly to the site of infection (respiratory tract). The first set of experiments used a multiple dosage regimen, in which the inhibitors were administered once daily for 7 consecutive days (Figure 5A and C). Compound **1** had a superior effect to ZNV at doses of 5 and 10 mg kg^{-1} and protected all mice from lethal virus challenge. In another experimental set that used a single-dose administration, all animals receiving ZNV at 20 mg kg^{-1} died within 9 days (Figure 5B and D). In contrast, the single treatment of **1** at an equivalent dosage provided 100% protection, demonstrating its prolonged effect. Pathological examination of mouse lung tissues at 7 days after infection indicated the pathology results correlated well with the antiviral treatments. Severe histological changes associated with bronchointerstitial pneumonia were detected in the untreated (Figure 5I) and uncured (Figure 5K and L) animals, whereas no appreciable lesions were

observed in compound **1**-treated mice that survived (Figure 5F and H) or in healthy controls (Figure 5E).

CONCLUSIONS

The superior in vivo efficacy of compound **1** over ZNV could be attributed to its improved binding with viral NA, and probably also to the increased molecular size that prolongs its residency in the respiratory tract,[47] as demonstrated by the divalent[26,27] and tetravalent[25] ZNV derivatives. The substantial increase in binding affinity, which arises from the simultaneous engagement of the inhibitor to all four active sites of the enzyme as designed, is important because it results in the efficient inhibition of both drug-sensitive and drug-resistant NAs. mutN2 and shaN9 used here contain either the E119V/I222L or R294K substitution that compromises the NA affinity of the drugs.[12,43] For example, the E119V mutation disrupts binding with the 4-guanidine of ZNV or the 4-amine of OSV, and R294K reduces the interaction with the carboxylate of both ZNV and OSV. The high activity of **1** against these mutant NAs demonstrates that the enhanced binding affinity compensated for the loss of interactions. Currently, drug-resistant strains with similar mutations to those used in this study are emerging.[5−8] Given the pandemic threat of resistant viruses, in addition to the fact that ZNV and OSV are the only two drugs recommended by the US Food and Drug Administration for worldwide use, the potent NA inhibitor **1**, with extended antiviral activities in both cell culture and animal models, represents a potential new treatment for influenza infection that may also be effective in controlling the current drug-resistant viral mutants. The success in targeting this tetravalent molecule to the surface of an enzyme tetramer suggests that this inhibitor design might be generally applicable to many proteins with multiple actives sites.

EXPERIMENTAL SECTION

General Chemistry Information. All chemical regents and solvents, including ZNV and OSV (in the form of oseltamivir carboxylate), were obtained from commercial source and used as purchased. TZs (**1**−**3**), **25**, and **29** were synthesized as described below. Other intermediate compounds were synthesized as described in the Support Information (in the section of Synthetic Protocols). Silica gel (100−200 mesh) for column chromatography was purchased from Qingdao Haiyang Chemical Co., Ltd (China). Sephadex G-15 was purchased from GE Healthcare (China). ^{1}H NMR (500 MHz) and ^{13}C NMR (125 MHz) spectra were measured on a Bruker Advance spectrometer. ESI-MS and ESI-HRMS spectra were recorded on a Bruker Apex IV FTMS spectrometer. The purity of final compounds is ≥95%, which was determined by an HPLC system (Agilent Technologies 1200) equipped with a UV detector using conditions as follows: Atlantis HILIC Silica columns (250 × 4.6 mm, 5 μm), 95→40%A (solvent A: 25% aqueous ammonia solution/acetonitrile (99:1, v/v), solvent B: 25% aqueous ammonia solution/deionized water (99:1, v/v)) gradient at 1 mL min^{-1} over 25 min, UV detection at 220 nm wavelength. The HPLC chromatograms for the analysis of TZs and compound **25** are provided in the Supporting Information (in the section of HPLC Chromatograms).

Tetravalent Zanamivir Conjugate (1). To a solution of compound **17** (120 mg, 0.024 mmol) in MeOH (2 mL) was added an aqueous solution of NaOH (1 M, 1 mL). The mixture was stirred at rt for 3 h, neutralized with Dowex 50 (H^+), filtered, and concentrated. The residue was dissolved in CH_2Cl_2/TFA (2 mL, 1:1, v/v). The mixture was stirred at rt for 3 h and concentrated. The resulting residue was dissolved in deionized water (0.5 mL) and filtered (Millipore Express 0.22 μM filter).

Purification with Sephadex G-15 (eluent: 0.1% TFA in H_2O) yielded **1** as a white solid (65.3 mg, 68%). mp 190−210 °C (with decomposition); $[\alpha]^{20}_D$ +28.6 (*c* 0.8, H_2O); ^{1}H NMR (500 MHz, D_2O): δ 8.16 (s, 4H, 4−HC=C−), 5.86 (d, *J* = 2.2 Hz, 4H, 4H-3), 4.86 (d, *J* = 8.9 Hz, 4H), 4.60 (s, 8H), 4.56 (s, 8H), 4.47 (d, *J* = 9.9 Hz, 4H), 4.35 (dd, *J* = 8.8, 2.0 Hz, 4H), 4.05 (t, *J* = 9.4 Hz, 4H), 3.93−3.90 (m, 4H), 3.63−3.56 (m, −OCH_2CH_2O−, 192H), 3.40−3.38 (m, 4H), 3.19−3.10 (m, 8H), 1.87 (s, 12H, 4NAc); ^{13}C NMR (125 MHz, D_2O): δ 173.8, 162.6, 156.9, 144.9, 128.0, 117.1, 115.1, 109.2, 75.5, 71.6, 69.6, 69.3, 68.7, 60.4, 47.1, 40.4, 22.1; ESI-HRMS: *m*/*z* calculated for $C_{165}H_{294}N_{32}O_{80}$ [M + 2H]$^{2+}$: 2001.9955, found: 2001.9908.

Tetravalent Zanamivir Conjugate (2). Using a procedure similar to that employed for the synthesis of **1**, deprotection of compound **18** (180 mg, 0.045 mmol) gave **2** as a white solid (103.4 mg, 78%). mp 180−200 °C (with decomposition); $[\alpha]^{20}_D$ +27.4 (*c* 0.8, H_2O); ^{1}H NMR (500 MHz, D_2O): δ 8.17 (s, 4H, 4−HC=C−), 5.94 (d, *J* = 2.5 Hz, 4H, 4H-3), 4.88 (dd, *J* = 8.9, 2.2 Hz, 4H), 4.61 (s, 8H), 4.57 (s, 8H), 4.50 (dd, *J* = 9.9, 2.1 Hz, 4H), 4.36 (dd, *J* = 8.9, 2.4 Hz, 4H), 4.06 (t, *J* = 9.4 Hz, 4H), 3.95−3.90 (m, 4H), 3.65−3.48 (m, 96H, −OCH_2CH_2O−), 3.43−3.39 (m, 4H), 3.26−3.10 (m, 8H), 1.88 (s, 12H, 4NAc); ^{13}C NMR (125 MHz, D_2O): δ 170.8, 162.0, 156.6, 152.8, 145.0, 144.6, 127.0, 109.8, 108.9, 83.6, 77.1, 70.6, 66.1, 64.4, 52.6, 41.1, 28.0; ESI-HRMS: *m*/*z* calculated for $C_{117}H_{198}N_{32}O_{56}$ [M + 2H]$^+$: 1473.6809, found: 1473.6816.

Tetravalent Zanamivir Conjugate (3). Using a procedure similar to that employed for the synthesis of **1**, deprotection of compound **19** (70 mg, 0.02 mmol) gave **3** as a white solid (36.7 mg, 76%). mp 160−180 °C (with decomposition); $[\alpha]^{20}_D$ +26.3 (*c* 0.8, H_2O); ^{1}H NMR (500 MHz, D_2O): δ 8.16 (s, 4H, 4−HC=C−), 5.86 (s, 4H, 4H-3), 4.86 (d, *J* = 8.5 Hz, 4H,), 4.60 (s, 8H), 4.56 (s, 8H), 4.47 (d, *J* = 10.2 Hz, 4H), 4.35 (d, *J* = 8.3 Hz, 4H), 4.05 (t, *J* = 9.4 Hz, 4H), 3.93−3.90 (m, 4H), 3.63−3.56

(m, 40H, −OCH_2CH_2O−), 3.48 (s, 8H), 3.40−3.38 (m, 4H), 3.19−3.10 (m, 8H), 1.87 (s, 12H, 4NAc); ^{13}C NMR (125 MHz, D_2O): δ 173.8, 165.2, 163.4, 157.0, 156.4, 145.5, 143.6, 127.8, 117.2, 114.9, 108.6, 75.7, 69.5, 69.3, 69.0, 68.7, 63.0, 62.4, 51.3, 50.1, 47.1, 40.1, 21.8; ESI-HRMS: *m*/*z* calculated for $C_{93}H_{150}N_{32}O_{44}$ $[M + 2H]^{2+}$: 1209.5236, found: 1209.5210.

Octavalent Zanamivir Conjugate (25). Click coupling[36] between compounds **24** and **14**, followed by a deprotection reaction, yielded **25**. Specifically, to a solution of compound **24** (10 mg, 8.6 μmol) and compound **14** (72 mg, 78 μmol) in THF/H_2O (1.5 mL, 2:1, v/v) was added a drop of aqueous solution of $CuSO_4$ (1 M) under a nitrogen atmosphere, followed by quick addition of sodium ascorbate (3.96 mg, 0.02 mmol). The mixture was stirred at 40 °C for 3 h and concentrated. The resulting residue was purified by silica gel column chromatography (CH_2Cl_2/MeOH 7:1, v/v) to give an intermediate compound as a white solid (30 mg, 3.5 μmol, 45%). Deprotection of this compound by a procedure similar to that employed for the synthesis of **1** gave **25** as a colorless oil (20.7 mg, 90% from intermediate compound, 37% from **24**); $[\alpha]^{20}_D$ +36.8 (*c* 0.8, H_2O); ^{1}H NMR (500 MHz, D_2O): δ 7.91 (s, 8H, 8−HC=C−), 5.51 (s, 8H, 8H-3), 4.74 (dd, J = 9.3, 1.5 Hz, 8H), 4.55 (s, 8H), 4.49 (s, 16H), 4.31 (m, 16H), 4.22 (dd, J = 9.2, 1.9 Hz, 8H), 3.88 (t, J = 9.8 Hz, 8H), 3.85 (m, 8H), 3.60−3.35 (m, 228H, −OCH_2CH_2O−), 3.30 (dd J = 11.7, 6.6 Hz, 20H), 3.23 (d, J = 17.5 Hz, 16H), 3.12 (m, 8H), 3.06 (m, 8H), 1.77 (s, 24H, 8NAc); ^{13}C NMR (125 MHz, D_2O): δ 173.8, 167.8, 156.9, 156.7, 148.6, 143.9, 143.1, 126.1, 124.1, 105.0, 76.7, 75.2, 69.5, 69.3, 69.1, 68.9, 68.5, 51.6; ESI-HRMS: *m*/*z* calculated for $C_{265}H_{453}N_{64}O_{128}Na$ $[M + Na]^+$: 6580.0905, found: 6582.0822.

Tetravalent OEG Conjugate (29). Using a procedure similar to that employed above in the click coupling reaction, compound **29** was afforded from **28** (131.8 mg, 0.28 mmol) and **16** (13 mg, 0.056 mmol) as a white solid (90.6 mg, 77%). ^{1}H NMR (500 MHz, $CDCl_3$): δ 8.14 (s, 4H,

4−HC=C−), 4.60 (s, 8H), 4.28 (s, 8H), 3.55−3.46 (m, 137H, −OCH_2CH_2O−), 3.44 (m, 8H), 3.28 (s, 12H, $4CH_3O$); ^{13}C NMR (125 MHz, $CDCl_3$): δ 144.8, 144.7, 131.0, 128.5, 126.8, 77.5, 77.2, 77.0, 71.8, 70.5, 69.9, 58.9; ESI-HRMS: *m*/*z* calculated for $C_{93}H_{177}N_{12}O_{40}$ $[M + H]^+$: 2102.2180, found: 2102.2178.

NAs, Viruses, Cells, and Animals. All NAs (N2, mutN2, shaN9, anhN9) were cloned, expressed, and purified as previously described.[12,19,37−42,48] For mutN2 that contained E119V and I222L, point mutations were introduced into the gene encoding the wild-type N2 (Generay Biotech, China). All viruses were generated using reverse genetics as previously described.[12,42,44−46] The A/Puerto Rico/8/34 (H1N1) virus was rescued from the genes of the natural isolate. The H3N2 virus contained the hemagglutinin gene and the NA gene of A/Moscow/10/99 (H3N2) with the remaining genes from A/Puerto Rico/8/34 (H1N1). The mutH3N2 virus had similar genes to the H3N2 virus, except for the mutant NA gene carrying E119V and I222L. The anhH7N9 and shaH7N9 viruses were produced from the genes of A/Anhui/1/2013 (H7N9) and H7N9 A/Shanghai/2/2013 (H7N9), respectively. MDCK cells were propagated in DMEM (Dulbecco's modified Eagle medium) containing 10% fetal calf serum, 100 U mL^{-1} penicillin, and 100 U mL^{-1} streptomycin, and maintained following known protocols.[49] The rescued viruses were amplified in MDCK cells. Viral culture supernatants were harvested, concentrated, and stored at −80 °C. The pfu and the $TCID_{50}$ (50% tissue culture infective dose) of viruses were quantified in MDCK cells. All experiments with the viruses were performed in approved biosafety level (BSL-3) containment laboratories. BALB/c mice and Sprague-Dawley rats were used for infection protection and pharmacokinetic experiments, respectively. Both were female and seven weeks old, and purchased from Vital River (China). All animals were used according to approved protocols for their care and use.

Computer Modeling. The known crystal structure of N9 NA in complex with ZNV (PDB code: 4MWX)[12] was used for computer simulation. The 3D structure of compound **1** was initially generated with ChemBio3D Ultra (version 11.0) and refined by running energy minimization with MOE (molecular operating environment, version 2014.09). The docking of **1** to N9 tetramer was carried out using MOE with standard program settings. Following the energy minimization of **1**−N9 complex, the free binding energy was calculated using a GBVI/WSA (generalized-born volume integral/weighted surface area) program in MOE. The free energy of ZNV binding to N9 monomer was also calculated similarly. Figure 1E was created with PyMOL (version 1.7.4).

NA Inhibition Assay. NA enzyme activity and competitive inhibition by inhibitor (OSV, ZNV, TZs, or compound **25**) were tested using MUNANA (4-methylumbelliferyl-*N*-acetylneuraminic acid) as a fluorescent substrate, according to published protocols.[12,19,38,50] In brief, NA activity was predetermined in an appropriate range (normally in 10−50 nM, in PBS) for fluorescence detection in the presence of MUNANA (167 μM, in PBS). For inhibition assays, the enzyme (10 μL) was mixed with serial 5-fold dilutions of inhibitor (10 μL, initial concentration at 1 mM) in PBS in a 96-well microplate and incubated at 37°C for 30 min. MUNANA (30 μL, 167 μM, in PBS) was then added to the mixture and fluorescence was measured on a SpectrMax M5 microplate reader (Molecular Devices), at excitation and emission wavelengths of 355 and 460 nm, respectively. Each assay was performed in no less than triplicates. IC_{50} values were determined with GraphPad Prism (version 5.0).

SPR Assay. The binding of inhibitor (ZNV or TZs) to NA (N2 or mutN2) were analyzed by a BIAcore T100 system (GE Healthcare, Sweden) based on SPR technique. NA was covalently immobilized on a CM5 sensor chip (research grade) by an amine-coupling method according to the

manufacturer's instructions. Five concentrations of inhibitor in PBS (10, 30, 90, 270 and 810 nM) were pre-prepared. The single-cycle kinetics protocol was used for SPR analysis. To each cycle, a solution of inhibitor was consecutively poured over the chip surface from low to high concentration at a flow rate of 40 μL min^{-1}. BSA and compound **29** were tested as negative controls instead of NA and inhibitor, respectively. Binding kinetic parameters were calculated using a steady affinity model with the BIAcore T100 analysis software (version 2.0.1).

X-ray Crystallography. Crystals of shaN9 were obtained by the vapour diffusion method from sitting drops as described previously.[12] Compound **1**−shaN9 complexes were prepared by soaking shaN9 crystals in crystallization solution (0.1 M HEPES, pH 7.5, containing 5% v/v 2-methyl-2,4-pentanediol and 10% v/v PEG 10,000) supplemented with 50 mM **1** at 4 °C for 3 h. The crystals were then flash-cooled at 100 K with cryoprotection. Diffraction data were collected on the beamline BL17U at Shanghai synchrotron radiation facility. The data were processed and scaled with HKL2000.[51] The structure of shaN9 in complex with **1** was determined by molecular replacement in Phaser using the CCP4 program suite,[52] with the known N9 NA structure (PDB code: 7NN9)[53] as a search model. Extensive model building was performed with Coot[54] and refined with Refmac.[55] Further refinement was done with phenix.refine implemented in the Phenix package.[56] The stereochemical quality of final model was validated with Procheck.[57] Figure 2F was produced with PyMOL. Crystallographic data and refinement statistics are provided in Table S3.

AUC Analysis. A solution of shaN9 in PBS (4.2 μM, 400 μL) was incubated at 37 °C for 3 h, in the absence or presence of inhibitor (1 mM solution of ZNV or compound **1** in PBS, 1.6 μL for 1 equiv assay and 9 μL for 5 equiv assay). The mixtures were then transferred into 400 μL sector-shaped 60Ti cells and scanned with a ProteomeLab XL-1 protein characterization system

(Beckman Coulter), at 20 °C, 230 nm, and the rotor speed of 40,000 rpm. Absorbance data were collected and analyzed with the SEDFIT software (version 9.4) to obtain the molecular weight distribution of shaN9.

In Vitro Viral Inhibition Assay. The in vitro antiviral activity of inhibitor (OSV, ZNV, **1**, **25**, or **29**) was determined in MDCK cell cultures. Serial 2-fold dilutions of inhibitor (initial concentration at 1 mM) in DMEM were prepared and mixed with an equal volume of virus (200 $TCID_{50}$) in the same medium. Following incubation at 37 °C for 1 h, the mixtures (100 μL) were added to MDCK cells, which were grown on 96-well microplates (10^4 cells per well). Further incubations (37 °C, under a 5% CO_2 atmosphere, 72 h) allowed for the inhibition of virus-induced cytopathic effects (CPEs) to be confirmed by microscopic examination. The virus titre in the infected cells was then determined with hemagglutination test and the EC_{50} values were calculated with the Reed and Muench method.[58,59] Four replicates were used for this viral inhibition assay.

Cytotoxicity Test. The cytotoxicity of inhibitor (OSV, ZNV, **1**, **25**, or **29**) on MDCK cells was measured using the standard procedure of MTT assay.[60]

TEM Examination. The H3N2 virus in DMEM (150 μL, 10^7 pfu) was incubated at 37 °C for 3 h, in the absence or presence of inhibitor (10 μL, 1 mM solution of ZNV, **1**, or **25** in PBS). The mixtures were then processed for TEM analysis (JEOL 1400) as described previously.[46]

Pharmacokinetic Analysis. Sprague-Dawley rats (n = 5) were given a single intravenous injection (in the tail vein) of inhibitor (ZNV or **1** in physiological saline) at a dosage of 6 μmol kg^{-1}. Blood sample collection and processing, inhibitor concentration measurement, and pharmacokinetic assessment were performed following the previously published method.[61] The HPLC conditions used to identify the inhibitors were as follows: (i) for ZNV: Ultimate C18/SCX column (5 μm, 2.1 × 100

mm), eluent A: 5 mM aqueous solution of ammonium acetate containing 0.1% v/v formic acid, eluent B: acetonitrile, 20→85%A gradient over 5 min at 0.6 mL min^{-1}; (ii) for compound **1**: ACQUITY CSH C18 column (1.7 μm, 2.1 × 50 mm), eluent A: deionized water containing 1% v/v ammonium hydroxide, eluent B: acetonitrile containing 1% v/v ammonium hydroxide, 10→95%A gradient over 5 min at 0.6 mL min^{-1}.

Mice Protection Experiments. Under anaesthesia, six mice per group were intranasally inoculated with the A/Puerto Rico/8/34 (H1N1) virus (10^5 pfu, in PBS, 40 μL). The inoculation was performed by dripping viral suspension into the nasal passages of mice with pipettes. For multiple-dose antiviral treatment, mice were intranasally administered with 5 or 10 mg kg^{-1} day^{-1} of the inhibitor (ZNV or **1** in PBS, 40 μL) for 7 days, starting at 1 day pi. For single-dose antiviral treatment, mice were treated only once with 20 mg kg^{-1} of inhibitor (ZNV or **1** in PBS, 40 μL) at 2 h pi. The infected control group was treated with 40 μL day^{-1} of PBS alone. All the treatments were performed by dripping antivirals or vehicles into the nasal passages of mice with pipettes. The mice (n = 6) without viral inoculation were used as the healthy control group. Body weight and survival of all mice were monitored for 14 days. Mice were accounted as dead when losing either 25% of their initial weight or when they were moribund. Figure 5A−D were created with the GraphPad Prism (version 5.0) on the basis of recorded data.

Pathological Examination. In mice protection experiments, one mouse per group was euthanized at 7 day pi, and the lung was harvest for pathological examinations. After immersion in 4% aqueous solutions of paraformaldehyde for 72 h, the excised tissues were processed for paraffin embedding and cut into 5 μm-thick sections, which were then stained using the standard

haematoxylin and eosin procedure. Pathological changes were examined with a Leica DM2500 upright metallurgical microscope.

Statistics. In mice protection experiments, statistically significant differences between the data of infected controls and those of inhibitor-treated groups were determined using Mantel-Cox test in GraphPad Prism (version 5.0).

ASSOCIATED CONTENT

Supporting Information

The Supporting Information is available free of charge on the ACS Publications website at DOI: Please insert doi number here.

Supplementary figures and tables, synthetic procedures and analytical data for intermediate compounds, NMR and MS spectra, HPLC chromatograms (PDF)

Accession Codes

Atomic coordinates and structure factors for the crystal structures of shaN9 in complex with compound **1** can be accessed using PDB codes: 5JYY. Authors will release the atomic coordinates and experimental data upon article publication.

AUTHOR INFORMATION

Corresponding Authors

*(X. Li) E-mail: lixb@im.ac.cn

*(G. F. Gao) E-mail: gaof@im.ac.cn

Author Contributions

⊥These authors contributed equally.

Notes

The authors declare no competing financial interest.

ACKNOWLEDGMENTS

The authors are grateful to Jinwei Ren (Institute of Microbiology, CAS) for technical help with the NMR experiments; Yuanyuan Chen and Zhenwei Yang (Institute of Biophysics, CAS) for technical help with the SPR experiments; Xiaoxia Yu (Institute of Biophysics, CAS) for technical help with the AUC experiments; Jingnan Liang (Institute of Microbiology, CAS) for technical help with the TEM analysis; Junfeng Hao and Guizhi Shi (Institute of Biophysics, CAS) for technical help with the pathological examination in the animal study. This work was funded by the Ministry of Science and Technology of China (973 program: 2012CB518803), the National Natural Science Foundation of China (programs: 31470801, 81273381, 21202195, 81301465 and 81330082), the Development Fund for Collaborative Innovation Center of Glycoscience of Shandong University, and the Open Project Program of National Engineering Research Center for Carbohydrate Synthesis, Jiangxi Normal University. Yan Wu is supported by Youth Innovation Promotion Association, CAS (program number: 2016086).

ABBREVIATIONS USED

AUC, analytical ultracentrifugation; CPE, cytopathic effect; DMEM, Dulbecco's modified Eagle medium; GBVI, generalized-born volume integral; HEPES,

4-(2-hydroxyerhyl)piperazine-1-erhanesulfonic acid; MDCK, Madin-Darby canine kidney; MOE, molecular operating environment; MTT, 3-(4,5-dimethylthiazol-2-yl)-2,5-diphenyltetrazolium bromide; MUNANA, 4-methylumbelliferyl-*N*-acetylneuraminic acid; NA, neuraminidase; OEG, oligoethylene glycol; OSV, oseltamivir; pi, postinfection; pfu, plaque forming units; SD, standard deviation; SPR, surface plasmon resonance; $TCID_{50}$, 50% tissue culture infective dose; TEM, transmission electron microscopy; TZ, tetravalent zanamivir; WSA, weighted surface area; ZNV, zanamivir

REFERENCES

(1) Liu, C.; Eichelberger, M. C.; Compans, R. W.; Air, G. M. Influenza type A virus neuraminidase does not play a role in viral entry, replication, assembly, or budding. *J. Virol.* **1995,** *69*, 1099−1106.

(2) von Itzstein, M.; Wu, W.-Y.; Kok, G. B.; Pegg, M. S.; Dyason, J. C.; Jin, B.; Phan, T. V.; Smythe, M. L.; White, H. F.; Oliver, S. W.; Colman, P. M.; Varghese, J. N.; Ryan, D. M.; Woods, J. M.; Bethell, R. C.; Hotham, V. J.; Cameron, J. M.; Penn, C. R. Rational design of potent sialidase-based inhibitors of influenza virus replication. *Nature* **1993,** *363*, 418−423.

(3) Kim, C. U.; Lew, W.; Williams, M. A.; Liu, H.; Zhang, L.; Swaminathan, S.; Bischofberger, N.; Chen, M. S.; Mendel, D. B.; Tai, C. Y.; Laver, W. G.; Stevens, R. C. Influenza neuraminidase inhibitors possessing a novel hydrophobic interaction in the enzyme active site: design, synthesis, and structural analysis of carbocyclic sialic acid analogues with potent anti-influenza activity. *J. Am. Chem. Soc.* **1997**, *119*, 681−690.

(4) von Itzstein, M. The war against influenza: discovery and development of sialidase inhibitors. *Nat. Rev. Drug Discovery* **2007,** *6*, 967−974.

(5) Kiso, M.; Mitamura, K.; Sakai-Tagawa, Y.; Shiraishi, K.; Kawakami, C.; Kimura, K.; Hayden, F. G.; Sugaya, N.; Kawaoka, Y. Resistant influenza A viruses in children treated with oseltamivir: descriptive study. *Lancet* **2004,** *364*, 759−765.

(6) Eshaghi, A.; Patel, S. N.; Sarabia, A.; Higgins, R. R.; Savchenko, A.; Stojios, P. J.; Li, Y.; Bastien, N.; Alexander, D. C.; Low, D. E.; Gubbay, J. B. Multidrug-resistant pandemic (H1N1) 2009 infection in immunecompetent child. *Emerg. Infect. Dis.* **2011,** *17*, 1472−1474.

(7) Le, Q. M.; Kiso, M.; Someya, K.; Sakai, Y. T.; Nguyen, T. H.; Nguyen, K. H. L.; Pham, N. D.; Ngyen, H. H.; Yamada, S.; Muramoto, Y.; Horimoto, T.; Takada, A.; Goto, H.; Suzuki, T.; Suzuki, Y.; Kawaoka, Y. Avian flu: isolation of drug-resistant H5N1 virus. *Nature* **2005,** *437*, 1108−1108.

(8) Hu, Y.; Lu, S.; Song, Z.; Wang, W.; Hao, P.; Li, J.; Zhang, X.; Yen, H.-L.; Shi, B.; Li, T.; Guan, W.; Xu, L.; Liu, Y.; Wang, S.; Zhang, X.; Tian, D.; Zhu, Z.; He, J.; Huang, K.; Chen, H.; Zheng, L.; Li, X.; Ping, J.; Kang, B.; Xi, X.; Zha, L.; Li, Y.; Zhang, Z.; Peiris, M.; Yuan, Z. Association between adverse clinical outcome in human disease caused by novel influenza A H7N9 virus and sustained viral shedding and emergence of antiviral resistance. *Lancet* **2013,** *381*, 2273−2279.

(9) Lackenby, A.; Hungnes, O.; Dudman, S. G.; Meijer, A.; Paget, W. J.; Hay, A. J.; Zambon, M. C. Emergence of resistance to oseltamivir among influenza A(H1N1) viruses in Europe. *Euro. Surveill.* **2008,** *13*, 8026.

(10) Bloom, J. D.; Gong, L. I.; Baltimore, D. Permissive secondary mutations enable the evolution of influenza oseltamivir resistance. *Science* **2010,** *328*, 1272−1275.

(11) Collins, P. J.; Haire, L. F.; Lin, Y. P.; Liu, J.; Russell, R. J.; Walker, P. A.; Skehel, J. J.; Martin, S. R.; Hay, A. J.; Gamblin, S. J. Crystal structures of oseltamivir-resistant influenza virus neuraminidase mutants. *Nature* **2008,** *453*, 1258−1261.

(12) Wu, Y.; Bi, Y.; Vavricka, C. J.; Sun, X.; Zhang, Y.; Gao, F.; Zhao, M.; Xiao, H.; Qin, C.; He, J.; Liu, W.; Yan, J.; Qi, J.; Gao, G. F. Characterization of two distinct neuraminidases from avian-origin human-infecting H7N9 influenza viruses. *Cell Res.* **2013,** *23*, 1347−1355.

(13) Yamashita, M.; Tomozawa, T.; Kakuta, M.; Tokumitsu, A.; Nasu, H.; Kubo, S. CS-8958, a prodrug of the new neuraminidase inhibitor R-125489, shows long-acting anti-influenza virus activity. *Antimicrob. Agents Chemother.* **2009,** *53*, 186−192.

(14) Kiso, M.; Kubo, S.; Ozawa, M.; Le, Q. M.; Nidom, C. A.; Yamashita, M.; Kawaoka, Y. Efficacy of the new neuraminidase inhibitor CS-8958 against H5N1 influenza viruses. *PLoS Path.* **2010**, *6*, e1000786.

(15) Shie, J.-J.; Fang, J.-M.; Wang, S.-Y.; Tsai, K.-C.; Cheng, Y.-S. E.; Yang, A.-S.; Hsiao, S.-C.; Su, C.-Y.; Wong, C.-H. Synthesis of tamiflu and its phosphonate congeners possessing potent anti-influenza activity. *J. Am. Chem. Soc.* **2007,** *129*, 11892−11893.

(16) Cheng, T.-J. R.; Weinheimer, S.; Tarbet, E. B.; Jan, J.-T.; Cheng, Y.-S. E.; Shie, J.-J.; Chen, C.-L.; Chen, C.-A.; Hsieh, W.-C.; Huang, P.-W.; Lin, W.-H.; Wang, S.-Y.; Fang, J.-M.; Hu, O. Y.-P.; Wong, C.-H. Development of oseltamivir phosphonate congeners as anti-influenza agents. *J. Med. Chem.* **2012**, *55*, 8657−8570.

(17) Schade, D.; Kotthaus, J.; Riebling, L.; Kotthaus, J.; Müller-Fielitz, H.; Raasch, W.; Koch, O.; Seidel, N.; Schmidtke, M.; Clement, B. Development of novel potent orally bioavailable oseltamivir derivatives active against resistant influenza A. *J. Med. Chem.* **2014**, *57*, 759−769.

(18) Rudrawar, S.; Dyason, J. C.; Rameix-Welti, M.-A.; Rose, F. J.; Kerry, P. S.; Russell, R. J. M.; van der Werf, S.; Thomson, R. J.; Naffakh, N.; von Itzstein, M. Novel sialic acid derivatives lock open the 150-loop of an influenza A virus group-1 sialidase. *Nat. Commun.* **2010**, *1*, 113.

(19) Vavricka, C. J.; Liu, Y.; Kiyota, H.; Sriwilaijaroen, N.; Qi, J.; Tanaka, K.; Wu, Y.; Li, Q.; Li, Y.; Yan, J.; Suzuki, Y.; Gao, G. F. Influenza neuraminidase operates via a nucleophilic mechanism and can be targeted by covalent inhibitors. *Nat. Commun.* **2013,** *4,* 1491.

(20) Kim, J.-H.; Resende, R.; Wennekes, T.; Chen, H.-M.; Bance, N.; Buchini, S.; Watts, A. G.; Pilling, P.; Streltsov, V. A.; Petric, M.; Liggins, R.; Barrett, S.; McKimm-Breschkin, J. L.; Niikura, M.; Withers, S. G. Mechanism-based covalent neuraminidase inhibitors with broad-spectrum influenza antiviral activity. *Science* **2013,** *340*, 71−75.

(21) Kerry, P. S.; Mohan, S.; Russell, R. J. M.; Bance, N.; Niikura, M.; Pinto, B. M. Structural basis for a class of nanomolar influenza A neuraminidase inhibitors. *Sci. Rep.* **2013**, *3*, 2871.

(22) Babu, Y. S.; Chand, P.; Bantia, S.; Kotian, P.; Dehghani, A.; El-Kattan, Y.; Lin, T.-H.; Hutchison, T. L.; Elliott, A. J.; Parker, C. D.; Ananth, S. L.; Horn, L. L.; Laver, G. W.; Montgomery, J. A. BCX-1812 (RWJ-270201): discovery of a novel, highly potent, orally active, and selective influenza neuraminidase inhibitor through structure-based drug design. *J. Med. Chem.* **2000**, *43*, 3482−3486.

(23) Abed, Y.; Simon, P.; Boivin, G. Prophylactic activity of intramuscular peramivir in mice infected with a recombinant influenza A/WSN/33 (H1N1) virus containing the H274Y neuraminidase mutation. *Antimicrob. Agents Chemother.* **2010**, *54*, 2819−2822.

(24) Honda, T.; Yoshida, S.; Arai, M.; Masuda, T.; Yamashita, M. Synthesis and anti-influenza evaluation of polyvalent sialidase inhibitors bearing 4-guanidino-Neu5Ac2en derivatives. *Bioorg. Med. Chem. Lett.* **2002**, *12*, 1929−1932.

(25) Watson, K. G.; Cameron, R.; Fenton, R. J.; Gower, D.; Hamilton, S.; Jin, B.; Krippner, G. Y.; Luttick, A.; McConnell, D.; MacDonald, S. J. F.; Mason, A. M.; Nguyen, V.; Tucker, S. P.; Wu, W.-Y. Highly potent and long-acting trimeric and tetrameric inhibitors of influenza virus neuraminidase. *Bioorg. Med. Chem. Lett.* **2004,** *14*, 1589−1592.

(26) Macdonald, S. J. F.; Watson, K. G.; Cameron, R.; Chalmers, D. K.; Demaine, D. A.; Fenton, R. J.; Gower, D.; Hamblin, J. N.; Hamilton, S.; Hart, G. J.; Inglis, G. G. A.; Jin, B.; Jones, H. T.; McConnell, D. B.; Mason, A. M.; Nguyen, V.; Owens, I. J.; Parry, N.; Reece, P. A.; Shanahan, S. E.; Smith, D.; Wu, W.-Y.; Tucker, S. P. Potent and long-acting dimeric inhibitors of influenza virus neuraminidase are effective at a once-weekly dosing regimen. *Antimicrob. Agents Chemother.* **2004**, *48*, 4542−4549.

(27) Macdonald, S. J. F.; Cameron, R.; Demaine, D. A.; Fenton, R. J.; Foster, G.; Gower, D.; Hamblin, J. N.; Hamilton, S.; Hart, G. J.; Hill, A. P.; Inglis, G. G. A.; Jin, B.; Jones, H. T.; McConnell, D. B.; McKimm-Breschkin, J.; Mills, G.; Nguyen, V.; Owens, I. J.; Parry, N.; Shanahan, S. E.; Smith, D.; Watson, K. G.; Wu, W.-Y.; Tucker, S. P. Dimeric zanamivir conjugates with various linking groups are potent, long-lasting inhibitors of influenza neuraminidase including H5N1 avian Influenza. *J. Med. Chem.* **2005**, *48*, 2964−2971.

(28) Tarbet, E. B.; Hamilton, S.; Vollmer, A. H.; Luttick, A.; Ng, W. C.; Pryor, M.; Hurst, B. L.; Crawford, S.; Smee, D. F.; Tucker, S. P. A zanamivir dimer with prophylactic and enhanced therapeutic activity against influenza viruses. *J. Antimicrob. Chemother.* **2014,** *69*, 2164−2174.

(29) Wen, W.-H.; Lin, M.; Su, C.-Y.; Wang, S.-Y.; Cheng, Y.-S. E.; Fang, J.-M.; Wong, C.-H. Synergistic effect of zanamivir-porphyrin conjugates on inhibition of neuraminidase and inactivation of influenza virus. *J. Med. Chem.* **2009**, *52*, 4903−4910.

(30) Varghese, J. N.; Laver, W. G.; Colman, P. M. Structure of the influenza virus glycoprotein antigen neuraminidase at 2.9 Å resolution. *Nature* **1983,** *303*, 35−40.

(31) Colman, P. M.; Varghese, J. N.; Laver, W. G. Structure of the catalytic and antigenic sites in influenza virus neuraminidase. *Nature* **1983,** *303*, 41−44.

(32) Kitov, P. I.; Sadowska, J. M.; Mulvey, G.; Armstrong, G. D.; Ling, H.; Pannu, N. S.; Read, R. J.; Bundle, D. R. Shiga-like toxins are neutralized by tailored multivalent carbohydrate ligands. *Nature* **2000,** *403*, 669−672.

(33) Kitov, P. I.; Bundle, D. R. On the nature of the multivalency effect: a thermodynamic model. *J. Am. Chem. Soc.* **2003,** *125*, 16271−16284.

(34) Spjut, S.; Qian, W.; Bauer,J.; Storm, R.; Frängsmyr, L.; Stehle, T.; Arnberg, N.; Elofsson, M. A potent trivalent sialic acid inhibitor of adenovirus type 37 infection of human corneal cells. *Angew. Chem. Int. Ed.* **2011,** *50*, 6519−6521.

(35) Harris, J. M.; Chess, R. B. Effect of pegylation on pharmaceuticals. *Nat. Rev. Drug Discovery* **2003,** *2*, 214−221.

(36) Rostovtsev, V. V.; Green, L. G.; Fokin, V. V.; Sharpless, K. B. A stepwise huisgen cycloaddition process: copper(I)-catalyzed regioselective "ligation" of azides and terminal alkynes. *Angew. Chem. Int. Ed.* **2002,** *41*, 2596−2599.

(37) Li, Q.; Qi, J.; Zhang, W.; Vavricka, C. J.; Shi, Y.; Wei, J.; Feng, E.; Shen, J.; Chen, J.; Liu, D.; He, J.; Yan, J.; Liu, H.; Jiang, H.; Teng, M.; Li, X.; Gao, G. F. The 2009 pandemic H1N1 neuraminidase N1 lacks the 150-cavity in its active site. *Nat. Struct. Mol. Biol.* **2010,** *17*, 1266−1268.

(38) Vavricka, C. J.; Li, Q.; Wu, Y.; Qi, J.; Wang, M.; Liu, Y.; Gao, F.; Liu, J.; Feng, E.; He, J.; Wang, J.; Liu, H.; Jiang, H.; Gao, G. F. Structural and functional analysis of laninamivir and its octanoate prodrug reveals group specific mechanisms for influenza NA inhibition. *PLoS Pathog.* **2011,** *7*, e1002249.

(39) Wu, Y.; Qin, G.; Gao, F.; Liu, Y.; Vavricka, C. J.; Qi, J.; Jiang, H.; Yu, K.; Gao, G. F. Induced opening of influenza virus neuraminidase N2 150-loop suggests an important role in inhibitor binding. *Sci. Rep.* **2013,** *3*, 1551.

(40) Li, Q.; Sun, X.; Li, Z.; Liu, Y.; Vavricka, C. J.; Qi, J.; Gao, G. F. Structural and functional characterization of neuraminidase-like molecule N10 derived from bat influenza A virus. *Proc. Natl. Acad. Sci. U. S. A.* **2012,** *109*, 18897−18902.

(41) Zhang, W.; Shi, Y.; Lu, X.; Shu, Y.; Qi, J.; Gao, G. F. An airborne transmissible avian influenza H5 hemagglutinin seen at the atomic level. *Science* **2013,** *340*, 1463−1467.

(42) Shi, Y.; Zhang, W.; Wang, F.; Qi, J.; Wu, Y.; Song, H.; Gao, F.; Bi, Y.; Zhang, Y.; Fan, Z.; Qin, C.; Sun, H.; Liu, J.; Haywood, J.; Liu, W.; Gong, W.; Wang, D.; Shu, Y.; Wang, Y.; Yan,

J.; Gao, G. F. Structures and receptor binding of hemagglutinins from human-infecting H7N9 influenza viruses. *Science* **2013,** *342*, 243−247.

(43) Richard, M.; Ferraris, O.; Erny, A.; Barthélémy, M.; Traversier, A.; Sabatier, M.; Hay, A.; Lin, Y. P.; Russell, R. J.; Lina, B. Combinatorial effect of two framework mutations (E119V and I222L) in the neuraminidase active site of H3N2 influenza virus on resistance to oseltamivir. *Antimicrob. Agents Chemother.* **2011,** *55*, 2942−2952.

(44) Wang, F.; Qi, J.; Bi, Y.; Zhang, W.; Wang, M.; Zhang, B.; Wang, M.; Liu, J.; Yan, J.; Shi, Y.; Gao, G. F. Adaptation of avian influenza A (H6N1) virus from avian to human receptor-binding preference. *EMBO J.* **2013,** *34*, 1661−1673.

(45) Bi, Y.; Xie, Q.; Zhang, S.; Li, Y.; Xiao, H.; Jin, T.; Zheng, W.; Li, J.; Jia, X.; Sun, L.; Qin, C.; Gao, G. F.; Liu, W. Assessment of the internal genes of influenza A (H7N9) virus contributing to high pathogenicity in mice. *J. Virol.* **2015,** *89*, 2−13.

(46) Wei, J.; Zheng, L.; Lv, X.; Bi, Y.; Chen, W.; Zhang, W.; Shi, Y.; Zhao, L.; Sun, X.; Wang, F.; Cheng, S.; Yan, J.; Liu, W.; Jiang, X.; Gao, G. F.; Li, X. Analysis of influenza virus receptor specificity using glycan-functionalized gold nanoparticles. *ACS Nano* **2014,** *8*, 4600−4607.

(47) Patton, J. S. Mechanisms of macromolecule absorption by the lungs. *Adv. Drug Delivery Rev.* **1996,** *19*, 3−36.

(48) Xu, X.; Zhu, X.; Dwek, R. A.; Stevens, J.; Wilson, I. A. Characterization of the 1918 influenza virus H1N1 neuraminidase. *J. Virol.* **2008**, *82*, 10493−10501.

(49) Hatakeyama, S.; Sakai-Tagawa, Y.; Kiso, M.; Goto, H.; Kawakami, C.; Mitamura, K.; Sugaya, N.; Suzuki, Y.; Kawaoka, Y. Enhanced expression of an alpha 2,6-linked sialic acid on MDCK

cells improves isolation of human influenza viruses and evaluation of their sensitivity to a neuraminidase inhibitor. *J. Clin. Microbiol.* **2005**, *43*, 4139−4146.

(50) Potier, M.; Mameli, L.; Belisle, M.; Dallaire, L.; Melancon, S. B. Fluorometric assay of neuraminidase with a sodium (4-methylumbelliferyl-alpha-D-N-acetylneuraminate) substrate. *Anal. Biochem.* **1979,** *94*, 287−296.

(51) Otwinowski, Z.; Minor, W. Processing of X-ray diffraction data collected in oscillation mode. *Methods Enzymol.* **1997**, *276*, 307−326.

(52) Read, R. J. Pushing the boundaries of molecular replacement with maximum likelihood. *Acta Crystallogr., Sect. D: Biol. Crystallogr.* **2001**, *57*, 1373−1382.

(53) Varghese, J. N.; Chandana Epa, V.; Colman, P. M. Three-dimensional structure of the complex of 4-guanidino-Neu5Ac2en and influenza virus neuraminidase. *Protein Sci.* **1995**, *4*, 1081−1087.

(54) Emsley, P. ; Cowtan, K. Coot: model-building tools for molecular graphics. *Acta Crystallogr., Sect. D: Biol. Crystallogr.* **2004**, *60*, 2126−2132.

(55) Murshudov, G. N.; Vagin, A. A.; Dodson, E. J. Refinement of macromolecular structures by the maximum-likelihood method. *Acta Crystallogr., Sect. D: Biol. Crystallogr.* **1997**, *53*, 240−255.

(56) Adams, P. D.; Afonine, P. V.; Bunkóczi, G.; Chen, V. B.; Davis, I. W.; Echols, N.; Headd, J. J.; Hung, L.-W.; Kapral, G. J.; Grosse-Kunstleve, R. W.; McCoy, A. J.; Moriarty, N. W.; Oeffner, R.; Read, R. J.; Richardson, D. C.; Richardson, J. S.; Terwilliger, T. C.; Zwart, P. H. PHENIX: a comprehensive python-based system for macromolecular structure solution. *Acta Crystallogr., Sect. D: Biol. Crystallogr.* **2010**, *66*, 213−221.

(57) Laskowski, R. A.; MacArthur, M. W.; Moss, D. S.; Thornton, J. M. SFCHECK: a unified set of procedures for evaluating the quality of macromolecular structure-factor data and their agreement with the atomic model. *J. Appl. Crystallogr.* **1993**, *26*, 283−291.

(58) Smee, D. F.; Huffman, J. H.; Morrison, A. C.; Barnard, D. L.; Sidwell, R. W. Cyclopentane neuraminidase inhibitors with potent in vitro anti-influenza virus activities. *Antimicrob. Agents Chemother.* **2001**, *45*, 743−748.

(59) Reed, L. J.; Muench, M. A simple method of estimating fifty percent end points. *Am. J. Hyg.* **1938**, *27*, 493−498.

(60) Mosmann, T. Rapid colorimetric assay for cellular growth and survival: application to proliferation and cytotoxicity assays. *J. Immunol. Methods* **1983**, *65*, 55−63.

(61) Cheng, S.; Chang, X.; Wang, Y.; Gao, G. F.; Shao, Y.; Ma, L.; Li, X. Glycosylated enfuvirtide: a long-lasting glycopeptide with potent anti-HIV activity. *J. Med. Chem.* **2015**, *58*, 1372−1379.

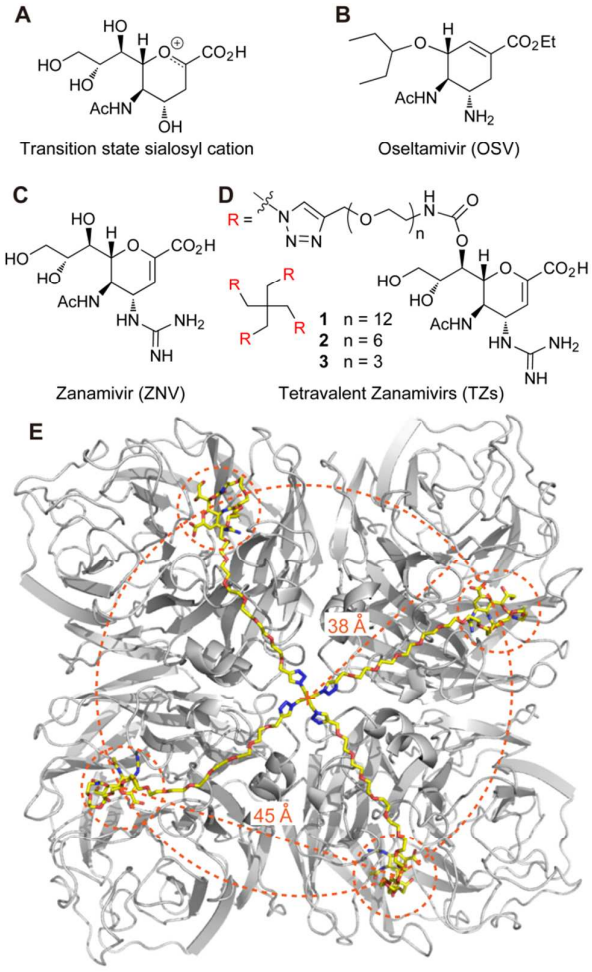

Figure 1. Sialic acid in transition state (A), OSV (B), ZNV (C), TZs (D), and a structural model of the NA tetramer in complex with **1** (E). In panel E, the NA tetramer (gray, PDB code: 4MWX) and compound **1** (yellow carbon, red oxygen, and blue nitrogen) are shown as a ribbon and stick representation, respectively. The dashed line indicates spatial arrangement of the active sites. In the refined conformation by computer simulation, each ZNV residue in **1**, **2**, and **3** is separated from the central carbon atom by 50, 30, and 18 Å, respectively. Thus, the molecular dimension of **1** has a better match of the NA active site distribution, whereas **2** and **3** are too small to bind all four subunits. However, compound **2** but not **3** can bridge two adjacent sites of the enzyme.

Scheme 1. Synthesis of TZs[a]

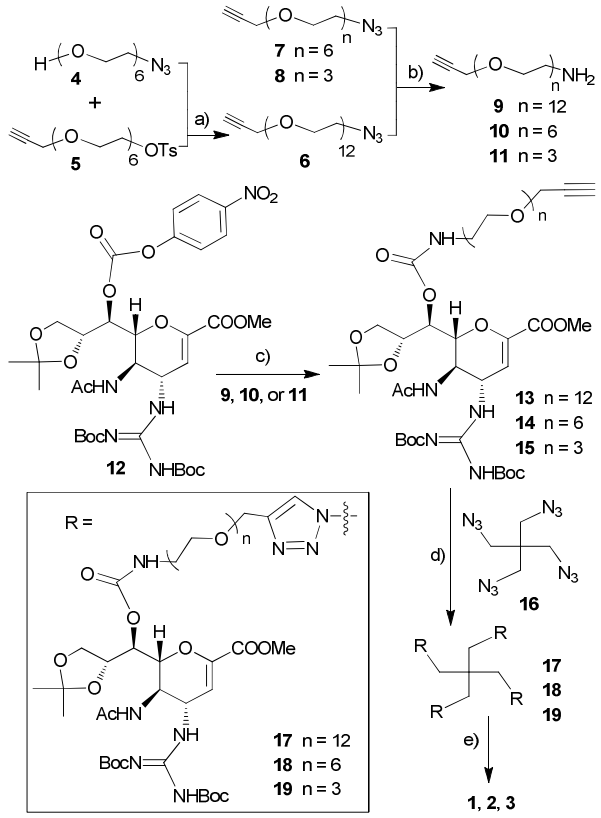

[a]A similar synthetic route has been reported previously.[29] Reaction conditions: (a) NaH, DMF, 80 °C, 36%; (b) Ph_3P, THF/H_2O (10:1), 45 °C, 86% for **9**; (c) DMAP, pyridine, rt, 64−86%; (d) $CuSO_4$ (1 M, in H_2O), sodium ascorbate, THF/H_2O (2:1), 40 °C, 74−83%; (e) i) MeOH, NaOH (1 M, in H_2O); ii) TFA in CH_2Cl_2 (50%), 68−78% (overall yield of two steps).

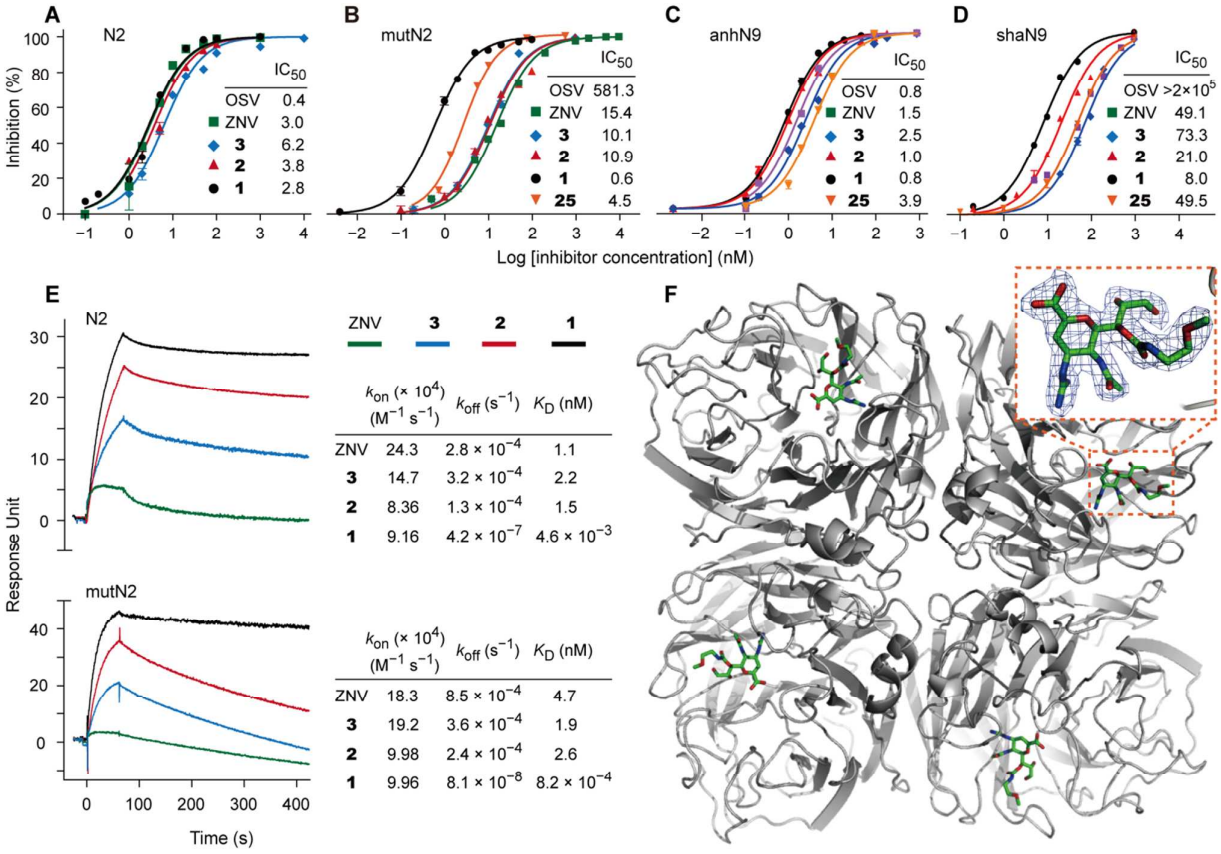

Figure 2. Analysis of interactions between NAs and TZs. (A−D) Inhibition of NA enzyme activity by TZs. IC_{50} values (nM) are the concentrations of inhibitor (OSV, ZNV, or ZNV residue in TZs and **25**) where the enzyme activity is reduced by 50%, and are shown as the means of triplicate assays (error estimates are provided in Table S1). OSV is used as its active form, oseltamivir carboxylate. The inhibitory curves of OSV are not shown. The inhibition of N2 by compound **25** is not determined. Error bars indicate standard deviation (SD). (E) Binding of TZs to N2 and mutN2 NAs analysed by a BIAcore biosensor system. The proteins were immobilized on the surface of SPR sensor chips. The analyte (TZs or ZNV) in running buffer at different concentrations was poured over the surface. The binding curves of analyte at 810 nM are shown. Kinetic data was calculated with the BIAcore analysis software, and are shown as the mean values from triplicate experiments (error estimates are provided in Table S2). (F) X-ray crystal structure of **1** bound to shaN9 tetramer

at a 2.1 Å resolution (PDB code: 5JYY). Only a single monomer of the binding complex was observed in electron density, and the tetrameric assembly is generated from crystallographic symmetry. This figure shows a top view of the structure. The side view is provided in Figure S2. The enzyme (gray) and inhibitor (carbon in green, oxygen in red, and nitrogen in blue) are shown. The ZNV residues of compound **1**, connecting with a short part of the linker, are clearly visible in $2F_o-F_c$ electron density (inset, contoured at 2.0σ). Crystallographic statistics are provided in Table S3.

Scheme 2. Synthesis of compounds 25 and 29[a]

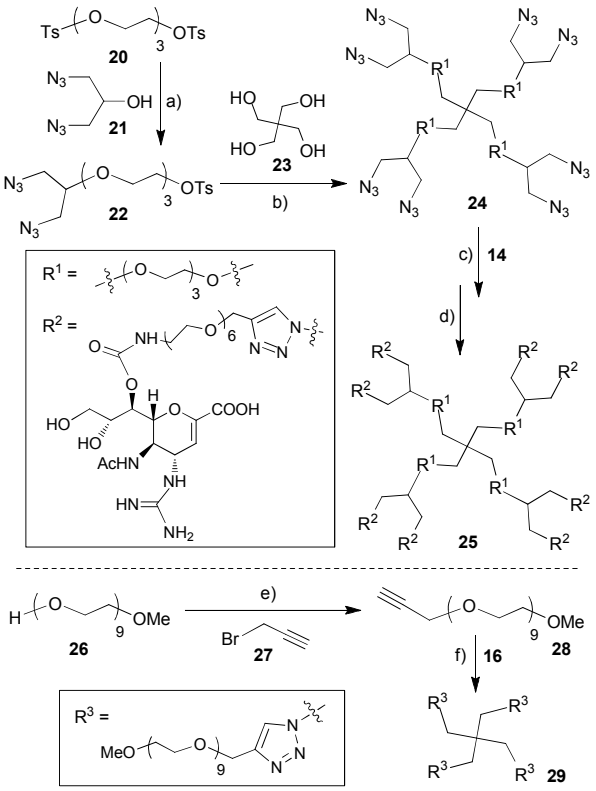

[a]Reaction conditions: (a) NaH, THF, 50 °C, 56%; (b) NaH, THF, 45 °C, 65%; (c) $CuSO_4$ (1 M, in H_2O), sodium ascorbate, THF/H_2O (2:1), 40 °C, 45%; (d) i) MeOH, NaOH (1 M, in H_2O); ii) TFA in CH_2Cl_2 (50%), 90%; (e) NaH, THF, 0→37 °C, 99%; (f) $CuSO_4$ (1 M, in H_2O), sodium ascorbate, THF/H_2O (2:1), 40 °C, 77%.

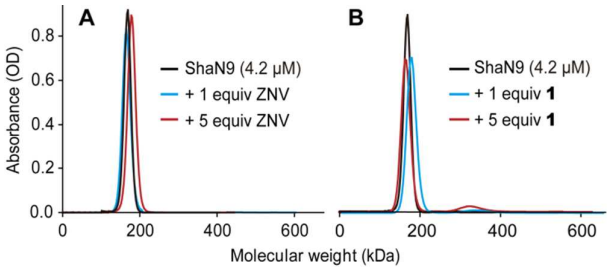

Figure 3. AUC analysis of shaN9 with added ZNV (A) or compound **1** (B). Single signals corresponding to the molecular weight of the shaN9 tetramer (~180 kDa) is observed for the enzyme alone or in the presence of ZNV. A major signal is also observed at 180 kDa in the presence of **1**, with few signs at approximately 360 kDa indicating that two NA tetramers are bridged by the compound.

Table 1. In Vitro Antiviral Activity of Compound 1

Virus[b]	EC_{50} (nM)[a]				
	OSV[c]	ZNV	**1**	**25**	**29**
H3N2	7.1 ± 0.7	17.7 ± 0.6	3.5 ± 0.3	2.7 ± 0.4	–[d]
mutH3N2	119.6 ± 13.3	154.5 ± 14.6	4.4 ± 0.3	7.7 ± 0.6	–
anhH7N9	12.3 ± 0.8	6.1 ± 0.7	1.2 ± 0.1	2.1 ± 0.1	ND[e]
shaH7N9	$>1.4 \times 10^5$	178.0 ± 15.3	7.1 ± 0.6	9.8 ± 0.8	ND

[a]EC_{50} refers to the concentration of inhibitor (OSV, ZNV, or ZNV residue in **1** and **25**) that causes a 50% reduction in viral replication in MDCK cells. All of assays were performed in quadruplicate and the results were reported as mean value ± SD. None of the inhibitors affected cell viability at concentrations below the micromolar range, as determined by MTT cytotoxicity assays. [b]H3N2, A/Moscow/10/99; mutH3N2, mutant A/Moscow/10/99 containing mutN2 NAs; anhH7N9, A/Anhui/1/2013; shaH7N9, A/Shanghai/2/2013. The mutH3N2 and shaH7N9 viruses are resistant to OSV and ZNV.[12,43] [c]Oseltamivir carboxylate. [d]No activity at concentrations below the micromolar range. [e]Not determined.

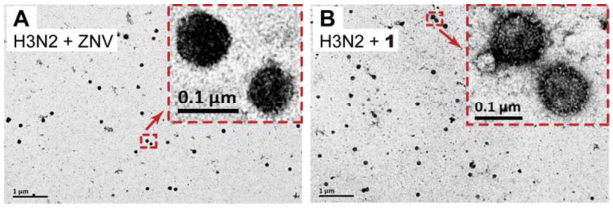

Figure 4. TEM images of H3N2 virus in the presence of ZNV (A) and compound **1** (B). The analyses were carried out after incubation of the virus (10^7 pfu, in DMEM, 150 µL) with **1** (1 mM, in PBS, 10 µL) for 3 hours. No apparent viral aggregations were observed ruling out the intervirion binding of the compound. TEM images of virus alone and in the presence of octavalent **25** are provided in Figure S4. Scale bars indicate 100 nm.

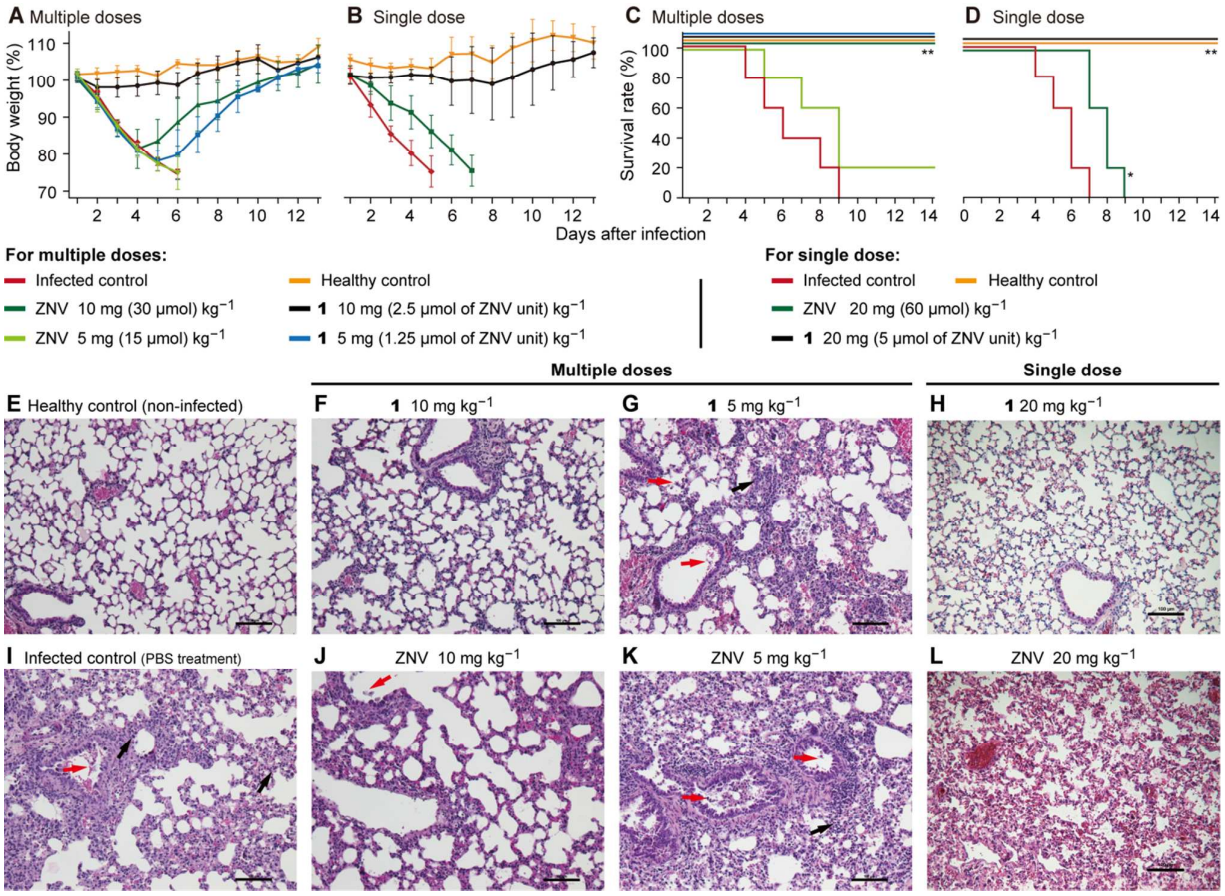

Figure 5. Protective efficacy of compound **1** against influenza infection in mice. BALB/c mice were intranasally inoculated with 10^5 plaque forming units (pfu) of A/Puerto Rico/8/34 (H1N1) virus. The infected mice were intranasally treated with **1**, ZNV, or PBS once daily for 7 consecutive days beginning at 1 d postinfection (pi) (A,C), or with a single dose of **1**, ZNV, or PBS at 2 h pi (B,D). PBS served as a control for antiviral treatments. Body weight (A,B) and survival (C,D) were monitored for 14 days. Mice were counted as dead when losing either 25% of their initial weight or when they were moribund. Statistical significance was determined by Mantel-Cox test (*$P < 0.05$, **$P < 0.01$). Error bars indicate SD. Six mice per group were used for assays and the lung tissue of one mouse from each group was harvested on 7 d pi for pathological examination (E−L, haematoxylin and eosin staining). Severe histological lesions characteristic of bronchointerstitial pneumonia were observed in infected controls (I) and the following treatment groups: 5 mg kg^{-1}

multiple-dose treatment by **1** and ZNV (G,K), and 20 mg kg^{-1} single-dose treatments by ZNV (L), with extensive bronchial wall thickening, immune cell infiltrates (black arrow), and respiratory epithelium desquamation (red arrow). Moderate lesions were found in the 10 mg kg^{-1} multiple-dose ZNV treatment group (J). No apparent pathological changes were observed in the 10 mg kg^{-1} multiple-dose (F) and 20 mg kg^{-1} single-dose (H) **1** treatment groups. Normal tissue without lesions is shown (E). Scale bars indicate 100 μm.

Table of Contents graphic